A&A 423, 579–592 (2004)
DOI: 10.1051/0004-6361:20041063

Astronomy & Astrophysics

Origin of diffuse C II 158 micron and Si II 35 micron emission in the Carina nebula⋆,⋆⋆

M. Mizutani[1,⋆⋆⋆], T. Onaka[1], and H. Shibai[2,3]

[1] Department of Astronomy, Graduate School of Science, University of Tokyo, Tokyo 113-0033, Japan
e-mail: onaka@astron.s.u-tokyo.ac.jp
[2] Division of Particle and Astrophysical Science, Graduate School of Science, Nagoya University, Nagoya 464-8602, Japan
[3] Institute of Advanced Research (IAR), Nagoya University, Nagoya 464-8602, Japan

Received 26 August 2003 / Accepted 11 May 2004

Abstract. We present the results of mapping observations with ISO of [O I] 63 μm, 145 μm, [N II] 122 μm, [C II] 158 μm, [Si II] 35 μm, and H_2 9.66 μm line emissions for the Carina nebula, an active star-forming region in the Galactic plane. The observations were made for the central $40' \times 20'$ area of the nebula, including the optically bright H II region and molecular cloud lying in front of the ionized gas. Around the center of the observed area is the interface between the H II region and the molecular cloud which creates a typical photodissociation region (PDR). The [C II] 158 μm emission shows a good correlation with the [O I] 63 μm emission and peaks around the H II-molecular region interface. The correlated component has the ratio of [C II] 158 μm to [O I] 63 μm of about 2.8. We estimate from the correlation that about 80% of [C II] emission comes from the PDR in the Carina nebula. The photoelectric heating efficiency estimated from the ratio of the ([C II] 158 μm + [O I] 63 μm) intensity to the total far-infrared intensity ranges from 0.06 to 1.2%. [O I] 145 μm is detected marginally at 10 positions. The average ratio of [O I] 145 μm to [O I] 63 μm of these positions is about 0.09 ± 0.01 and is larger than model predictions. The observed [C II] 158 μm to [O I] 63 μm ratio indicates a relatively low temperature (<500 K) of the gas, while the large [O I] 145 μm to 63 μm ratio suggests a high temperature (~1000 K). This discrepancy cannot be accounted for consistently by the latest PDR model with the efficient photoelectric heating via polycyclic aromatic hydrocarbons (PAHs) even if absorption of [O I] 63 μm by foreground cold gas is taken into account. We suggest that absorption of [C II] 158 μm together with [O I] 63 μm by overlapping PDRs, in which the heating via PAHs is suppressed due to the charge-up effect, may resolve the discrepancy. Quite strong [Si II] 35 μm emission has been detected over the observed area. It shows a good correlation with [N II] 122 μm, but the correlation with [O I] 63 μm is very weak, indicating that [Si II] 35 μm comes mainly from the diffuse ionized gas rather than the PDR. The ratio of [Si II] 35 μm to [N II] 122 μm is about 8 and Si of about 50% of the solar abundance relative to *N* should be present in the gas phase. The present results suggest that efficient dust destruction takes place and a large fraction of Si returns to the gas in the Carina star-forming region.

Key words. infrared: ISM – ISM: abundances – ISM: individual objects: Carina nebula – ISM: lines and bands – ISM: dust, extinction

1. Introduction

The surface of molecular clouds irradiated by strong far-ultraviolet (FUV) photons (6 eV< $h\nu$ < 13.6 eV), which control the heating and gas phase chemistry, is an interesting region for the study of the interstellar medium (ISM). Known as photodissociation regions (PDR), these regions emit strongly in the far-infrared (FIR) through the atomic fine-structure and molecular emission lines and thermal dust continuum emission. Several models have been constructed to interpret the molecular and atomic emissions together with the FIR continuum emission observed in PDRs (e.g. de Jong et al. 1980; Tielens & Hollenbach 1985; Wolfire et al. 1990; Hollenbach et al. 1991; Le Bourlot et al. 1993; Kaufman et al. 1999; Mochizuki & Nakagawa 2000; for a review, Hollenbach & Tielens 1999). In these models FIR line emission plays an important role in the energy balance and provides useful tools for diagnostics of the physical conditions and investigations of the heating and cooling mechanisms. Major cooling lines in PDRs, such as [O I] 63 μm, 145 μm, [C II] 158 μm, and [Si II] 35 μm, have been observed in various objects, including the Galactic center,

⋆ Based on observations with ISO, an ESA project with instruments funded by ESA Member States (especially the PI countries: France, Germany, The Netherlands and the United Kingdom) and with the participation of ISAS and NASA.
⋆⋆ Table 2 is only available in electronic form at the CDS via anonymous ftp to cdsarc.u-strasbg.fr (130.79.128.5) or via http://cdsweb.u-strasbg.fr/cgi-bin/qcat?J/A+A/423/579
⋆⋆⋆ *Present address:* Central Research Laboratory, Hitachi, Ltd., 1-280 Higashi-Koigakubo, Kokubunji, Tokyo 185-8601, Japan.

H II regions, molecular clouds, and external galaxies, and they have provided significant information for the study of the physical nature of the objects (e.g., Erickson et al. 1991; Meixner et al. 1992; Colgan et al. 1993; Carral et al. 1994; Tauber et al. 1994; Stolovy et al. 1995; Lord et al. 1996; Poglitsch et al. 1996; Colbert et al. 1999; Liseau et al. 1999; Unger et al. 2000; Vastel et al. 2001; Negishi et al. 2001; Malhotra et al. 2001; Young Owl et al. 2002; Okada et al. 2003).

The [C II] 158 μm line is one of the major cooling lines in PDRs and has been detected in a wide range of objects as well as in the diffuse Galactic emission (e.g., Crawford et al. 1985; Matsuhara et al. 1989; Shibai et al. 1991, 1996; Wright et al. 1991; Bock et al. 1993; Yui et al. 1993; Stacey et al. 1991, 1993; Nakagawa et al. 1998; Makiuti et al. 1996, 2002; Li et al. 2002). C^+ ions exist in regions where hydrogen is neutral or ionized because the ionization potential (11.26 eV) is less than that of hydrogen. Since the [C II] 158 μm transition is relatively easily excited by electrons (see Table 1), a significant fraction of the [C II] 158 μm emission is expected to come also from H II regions. It is thus important to correctly estimate the contribution to [C II] 158 μm from the ionized gas for the study of physical conditions of PDRs.

Si^+ can also be emitted in regions of either neutral or ionized hydrogen since its ionization potential is only 8.15 eV. The [Si II] 35 μm emission has been observed in several H II regions (Haas et al. 1991; Peeters et al. 2002) and reflection nebulae (Young Owl et al. 2002), as well as in the Galactic center direction (Erickson et al. 1991; Stolovy et al. 1995). Intense [Si II] 35 μm emissions detected in a starburst galaxy and a star-forming region have been interpreted in terms of significantly enhanced Si in the gas phase in H II regions and/or PDRs compared to the cold neutral medium (Carral et al. 1994; Okada et al. 2003). Silicon is a major constituent of interstellar dust grains (Mathis 1990). The large gas phase abundance of Si in PDRs or in H II regions suggests efficient grain destruction occurring in these regions. Hence, investigations on the origin of the diffuse [C II] 158 μm and [Si II] 35 μm emissions are of great importance for the study of physical conditions and dust processing in the ISM.

There have been a large number of observations carried out with the Kuiper Airborne Observatory (KAO) for the study of the ISM. However these observations were made with different instruments and at different times for each line emission in most cases. The Long Wavelength Spectrometer (LWS; Clegg et al. 1996) and Short Wavelength Spectrometer (SWS; de Graauw et al. 1996) on board the Infrared Space Observatory (ISO; Kessler et al. 1996) provided a unique capability of efficient observations of the whole spectra at FIR wavelengths with much higher sensitivities than previous observations. The wide wavelength coverage enables us to investigate the nature of the ISM in detail. Combined SWS and LWS spectra give us a great deal of information on the emitting gas and dust as demonstrated for H II regions by Peeters et al. (2002) and Martín-Hernández et al. (2002).

The Carina nebula is one of the most active star-forming regions in the Galactic plane. It contains two H II regions, Car I and Car II which are excited by the massive star clusters, Trumpler (Tr) 16 and Tr 14, respectively. Numerous O-type stars, including the most massive O3 stars, and several Wolf-Rayet stars are present in the star clusters (Feinstein 1995; Walborn 1995). The extreme excitation conditions and the stellar winds from these massive stars have deeply affected the surroundings, making the Carina nebula a very prominent region in the Galaxy. The brightest peculiar object in the infrared, η Car, is also a member of Tr 16 (Morris et al. 1999). The bright nebulosity and prominent dust lane are seen in visual images. The large-scale structure of the Carina cloud complex has been investigated in various wavelengths (Cox 1995 for a review of previous work). It has recently been investigated in detail by CO($J = 1 - 0$) observations (Brooks et al. 1998), near- to mid-infrared observations (Smith et al. 2000; Rathborne et al. 2002), and CO ($J = 4$–3) and [C I] $^3P_1 - ^3P_0$ transitions (Zhang et al. 2001). The H II region is partly covered with the molecular cloud, which causes the obscuration seen in the dust lane (de Graauw et al. 1981). The interface region between the H II region and molecular cloud forms a typical PDR (Brooks et al. 2003). Infrared spectroscopy of this highly excited region should provide useful information on the physical conditions and the elemental abundance in this active region.

In this paper, we report mapping observations of the Carina nebula with the LWS and SWS. In a previous paper we reported the results of the analysis of highly ionized ionic lines of [O III] 52, 88 μm, and [N III] 57 μm and indicated the presence of highly-ionized diffuse gas of low electron density extending around the Carina nebula region (Mizutani et al. 2002, hereafter Paper I). Here we report the results and analysis on four major emission lines in PDRs, [O I] 63, 145 μm, [C II] 158 μm, and [Si II] 35 μm, as well as [N II] 122 μm and H_2 9.66 μm lines. The intensities of the [N II] 122 μm emission are given in Paper I and the analysis is given in the present paper. [N II] 122 μm originates from the low-density diffuse ionized gas and provides a good measure for estimating the contribution from the ionized gas to the [C II] 158 μm and [Si II] 35 μm emissions. The parameters of these lines are summarized in Table 1.

2. Observations and data reduction

The observations were made for the $40' \times 20'$ area in the Carina nebula centered at $(l, b) = (287.^\circ4, -0.^\circ6)$. Two O-type star clusters Tr 14 and 16, the H II regions Car I and II, and the associated molecular cloud were included in the observed area (see Paper I for details). The LWS observations were executed in the LWS01 full grating scan mode (45–170 μm, $\lambda/\Delta\lambda = 100$–$300$). The mapping observations consist of six raster scans and the spectra were obtained at 132 positions with a $3'$ grid. Among them 8 positions were observed twice, for which the data were averaged. Thus we finally have the data at 124 positions. The observed area consists of two parts. One is the main mapping area ($287.^\circ0 \le l \le 287.^\circ65$, $-0.^\circ8 \le b \le -0.^\circ4$), where the observations were made at 12×8 positions. The additional 12×2 spositions parallel to the Galactic plane ($287.^\circ05 \le l \le 287.^\circ6$, $-0.^\circ34 \le b \le -0.^\circ28$) were also observed. Figure 1 shows a visual image of the Carina region from the

Table 1. Parameters for the fine-structure lines analyzed in the present paper.

Species	Ionization potential[a] (eV)	Wavelength (μm)	Transition	A-coefficient[b] (s^{-1})	Collision partner	Critical density[b] (cm^{-3})
O I	–	63.1837	$^3P_1 - ^3P_2$	8.95×10^{-5}	H	1.6×10^7
					e	3.2×10^4
		145.5254	$^3P_0 - ^3P_1$	1.70×10^{-5}	H	1.3×10^6
					e	7.4×10^3
N II	14.53	121.8	$^3P_2 - ^3P_1$	7.46×10^{-6}	e	380
C II	11.26	157.7408	$^2P_{3/2} - ^2P_{1/2}$	2.29×10^{-6} [c]	e	40[d]
					H	2.8×10^3[d]
Si II	8.15	34.814	$^2P_{3/2} - ^2P_{1/2}$	2.17×10^{-4}	H	2.6×10^5
					e	1.4×10^3[e]

[a] The ionization potentials are taken from Allen (1973).
[b] The A-coefficients and critical densities are taken from Mendoza (1983) otherwise mentioned. The critical densities are estimated with $T = 10\,000$ K for electron and with $T = 100$ K for hydrogen atom.
[c] The A-coefficient of [C II] 158 μm is taken from Nussbaumer & Storey (1981).
[d] The critical density of [C II] 158 μm is taken from Launey & Roueff (1977) for H and Hayes & Nussbaumer (1984) for electron.
[e] The critical density of [Si II] 35 μm for electron is calculated for $T = 10\,000$ K with the collision strength from Osterbrock (1989).

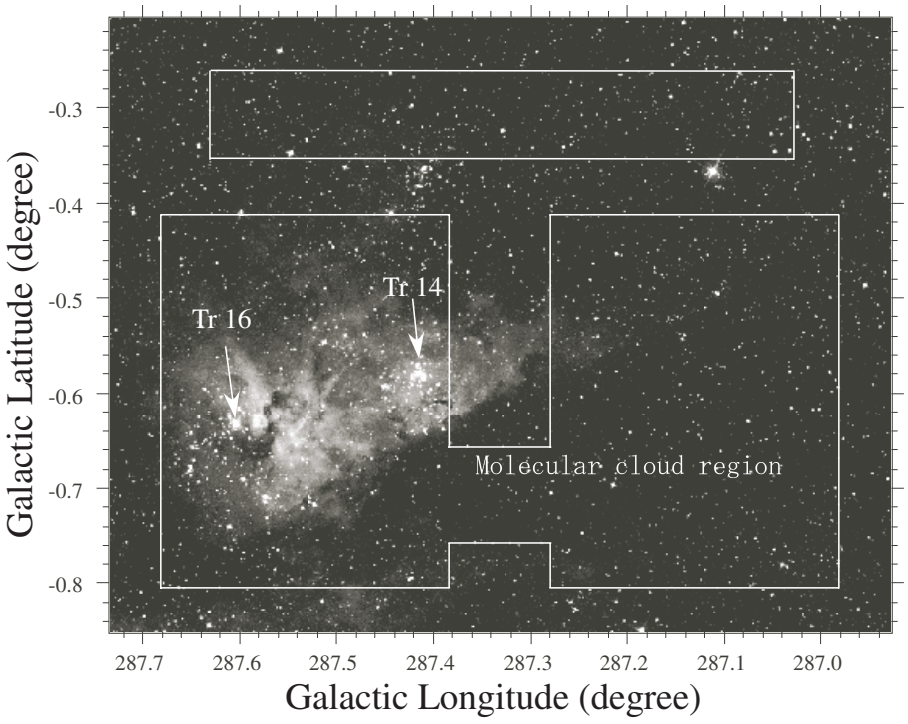

Fig. 1. Visual image of the observed region from the Digital Sky Survey. The area for which the LWS observations were carried out is enclosed by white lines. The bright part in the left indicates H II regions, while the lower right area is the molecular gas regions.

Digital Sky Survey[1], on which the area observed by the LWS is enclosed by white lines. There is a T-shaped area where the observations were not executed. Additional 4 positions in the outer region were also observed (Paper I), but their data are not used in the present study. Four grating scans were executed at each raster position and the total integration time was 2 s at each grating position. The spectral sampling was made with a half of the resolution element. The LWS aperture depends on the wavelength and is approximately 80″ (Gry et al. 2002).

The same area was observed with the SWS grating line-profile scan mode (SWS02). The SWS observations were made in the wavelength ranges 34.6–35.2 μm (LW section, band 4C) for the [Si II] $^2P_{3/2} - ^2P_{1/2}$ transition at 34.8 μm and 9.61–9.72 μm (SW section, band 2C) for the H_2 $J = 5$–3 pure rotational transition at 9.66 μm. The aperture sizes were 20″ × 33″ and 14″ × 20″, respectively, and the spectral

[1] Based on photographic data of the National Geographic Society – Palomar Observatory Sky Survey (NGS-POSS) obtained using the Oschin Telescope on Palomar Mountain. The NGS-POSS was funded by a grant from the National Geographic Society to the California Institute of Technology. The plates were processed into the present compressed digital form with their permission. The Digitized Sky Survey was produced at the Space Telescope Science Institute under US Government grant NAG W-2166.

resolutions about 1500 at 35 μm and 2000 at 9.6 μm (Leech et al. 2002). The SWS observations were made for the same positions as those observed with the LWS except for the central strip. They were executed as the concatenated observations and the total integration time for each position was 200 s. The difference between the corresponding positions of the LWS and SWS is less than 0.°01. Both the LWS and SWS observations were made with the spatial interval of 3′, larger than their apertures, providing undersampled maps.

In the present study we used the LWS data of the Off-Line Processing (OLP) version 8 as in Paper I. The post pipeline processing was performed with our own software developed based on the ISO spectral analysis package (ISAP[2]), in which the remaining glitches were removed and the fringing pattern was corrected. The spectra were rebinned and averaged over 4 scans. Then the extended source correction was applied with the latest correction factors and beam sizes given in Gry et al. (2002). In the SWS data reduction, the products of the OLP version 9 were used. The spectra were reduced by using the SWS Interactive Analysis (IA) software as of December 1999 provided by the SWS Instrument Dedicated Team (IDT). We applied the flux conversion factors for extended sources reported by Salama (2000). Because the SWS spectra were taken in the early stage of the ISO mission, the dark current measurements were not executed in the optimum manner. The offset levels of the spectra could not be well determined due to large uncertainties in the dark current estimates. However, they do not affect the derivation of the intensity of emission lines.

The line intensities were derived by Gaussian fitting. The baseline for each line emission was estimated by fitting the nearby continuum with a straight line. The error in the line intensity was estimated including the uncertainty in the baseline (see Paper I for details). The uncertainty in the absolute calibration for the LWS is estimated to be 10–20% for point sources and 50% for extended sources (Gry et al. 2002). The flux calibration uncertainty in the SWS is 7% and 22%, for the H_2 9.66 μm and [Si II] 35 μm lines, respectively and the uncertainty in the conversion factors for extended sources is less than 10% (Leech et al. 2002).

Examples of the spectra at three positions, north of η Car, the interface region, and the molecular region, $((l, b)$ = (287.°61, −0.°59), (287.°41, −0.°54), and (287.°11, −0.°69)), are displayed in Fig. 2. Each spectrum for H_2 9.66 μm, [Si II] 35 μm, and LWS is plotted in the same scale for the three positions. The offset levels of the SWS spectra are arbitrary because of the uncertainty in the dark current measurements.

The LWS continuum spectrum was fitted with a single-temperature graybody function to estimate the total FIR intensity FIR and the intensity of the incident radiation field G_0. First the flux level for each detector channel was scaled to the SW2 channel to correct the gaps between the channels and the individual spectra were stitched. The SW2 channel was chosen as a reference because it provided an average signal level among the 10 channels for most observed positions. The scaling factors were in the range 0.7–1.3. The resulting spectrum was fitted with a function $\tau_{100}(100\,\mu\mathrm{m}/\lambda)^{\beta}B_{\lambda}(T)$, where $B_{\lambda}(T)$ is the Planck function of the temperature T and τ_{100} is the optical depth at 100 μm. The power law index of the emissivity β was fixed as unity because it gave the best fit. FIR is then estimated as

$$FIR = \tau_{100}\int_0^{\infty} B_{\lambda}(T)(100\,\mu\mathrm{m}/\lambda)\mathrm{d}\lambda. \quad (1)$$

From the energy balance we estimate the incident radiation intensity G_0 in units of the solar neighborhood value, 1.6×10^{-6} W m^{-2} (Habing 1968), as

$$G_0 = \frac{1}{\langle\tau_{\mathrm{abs}}\rangle}\frac{4\pi FIR}{1.6\times10^{-6}\,\mathrm{W m^{-2}}}, \quad (2)$$

where $\langle\tau_{\mathrm{abs}}\rangle$ is the absorption optical depth averaged over the incident radiation spectrum. The incident radiation intensity G_0 is a function of T ($\propto T^5$) and we assume $\langle\tau_{\mathrm{abs}}\rangle/\tau_{100} = 700$ (Chan et al. 2001). The absolute uncertainty in FIR is estimated to be 50% from the absolute calibration uncertainty of

Table 3. Line intensity in the central strip observed by SWS.

Position		Intensities[a] (10^{-8} W m^{-2} sr^{-1})			
l	b	[Si II] 35 μm		H_2 9.66 μm	
287.306	−0.636	85.9	(13.0)	17.1	(2.2)
287.306	−0.786	49.0	(8.0)	<0.8	
287.356	−0.786	29.7	(5.7)	<1.5	
287.356	−0.636	210.7	(29.6)	12.9	(1.7)
287.306	−0.586	108.4	(15.9)	<1.6	
287.306	−0.536	49.8	(7.5)	<1.1	
287.306	−0.486	11.7	(2.3)	<0.9	
287.306	−0.436	9.9	(2.4)	<1.2	
287.306	−0.386	13.6	(2.8)	<0.9	
287.306	−0.236	10.3	(2.8)	<0.7	
287.306	−0.186	13.1	(3.7)	<0.9	
287.306	−0.136	9.8	(3.2)	<0.4	
287.306	−0.086	14.8	(3.3)	<0.8	
287.306	−0.036	10.4	(3.3)	<0.9	
287.356	−0.036	16.4	(3.7)	<1.5	
287.356	−0.086	16.3	(3.3)	<1.3	
287.356	−0.136	13.9	(2.9)	<1.0	
287.356	−0.186	8.4	(2.2)	<1.0	
287.356	−0.236	8.8	(1.6)	<0.5	
287.356	−0.386	13.4	(2.9)	<0.9	
287.356	−0.436	12.3	(3.1)	<1.1	
287.356	−0.486	23.6	(4.1)	<0.6	
287.356	−0.536	53.5	(8.1)	<1.3	
287.356	−0.586	99.8	(15.1)	13.8	(1.7)
287.306	−0.497	<0.6		<1.4	
287.356	−0.497	<0.4		<0.6	
287.306	−0.831	<0.4		<0.4	
287.356	−0.831	<0.7		<1.5	

[a] The numbers in the parentheses indicate the statistical errors (1σ) and the uncertainty in the absolute calibration is not included.

[2] The ISO Spectral Analysis Package (ISAP) is a joint development by the LWS and SWS Instrument Teams and Data Centers. Contributing institutes are CESR, IAS, IPAC, MPE, RAL and SRON.

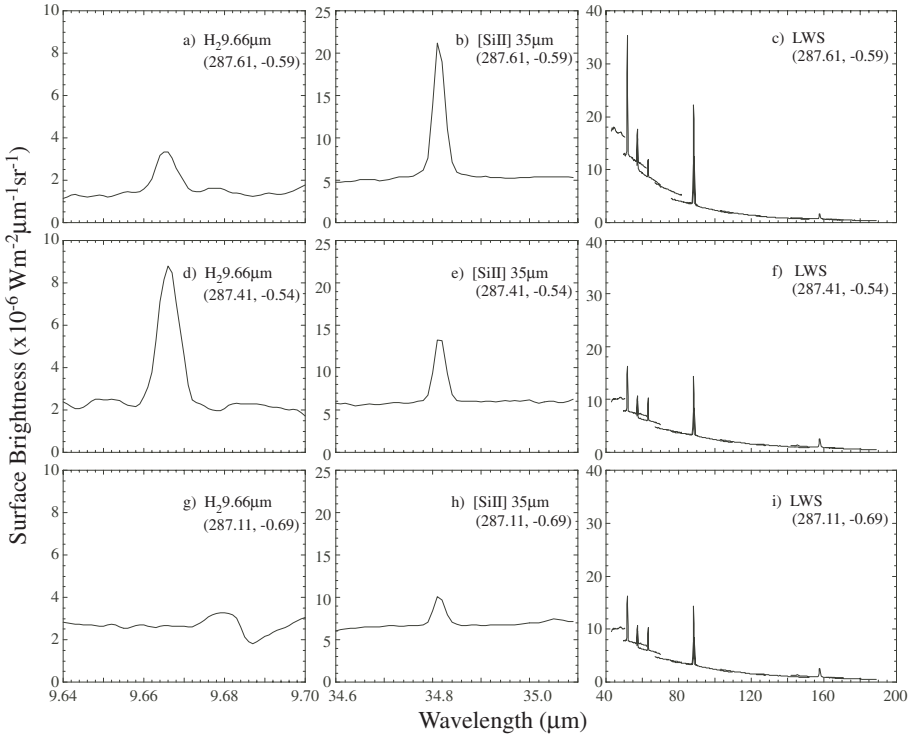

Fig. 2. Sample spectra of three positions. The top three panels **a)**, **b)**, and **c)** are the H_2 9.66 μm, [Si II] 35 μm, and LWS spectra, respectively, at north of η Car ((l, b) = (287.°61, −0.°59)), the middle panels **d)**, **e)** and **f)** are those near the interface region ((l, b) = (287.°41, −0.°54)), and the bottom panels **g)**, **h)**, and **i)** are those towards the molecular region ((l, b) = (287.°11, −0.°69)). Each spectrum for H_2 9.66 μm **a)**, **d)**, and **g)**, [Si II] 35 μm **b)**, **e)**, and **h)** and LWS **c)**, **f)**, and **i)** is plotted in the same scale for the three positions. The offset levels of the SWS spectra **a)**, **b)**, **d)**, **e)**, **g)**, and **h)** are arbitrary because of the uncertainty in the dark current measurements.

the LWS. The relative accuracy, such as the ratios between line intensities and *FIR*, is estimated to be better than 30% from the gaps between the signal levels of the detectors. In the observed region G_0 ranges from 400 to 5000 (see Fig. 5). The radiation field strength G_0 can also be estimated from the stellar properties in Tr 14 and Tr 16 (Walborn 1973; Vázquez et al. 1996; Brooks et al. 2003). Neglecting dust absorption and projection effects, G_0 estimated from the stellar properties is about 10^4 around the interface region, while G_0 from Eq. (2) indicates $(5-8)\times10^3$ in the same region. The present results are in agreement with Brooks et al. (2003), who estimated $G_0 \sim 10^4$ for the PDR associated with Tr 14. The G_0 values estimated from the stellar properties and Eq. (2) agree with each other fairly well in the outer part of the observed region ($G_0 \sim 400-1000$). The derived value of G_0 includes the contribution from photons with $E < 6$ eV and does not exactly correspond to the UV radiation field strengths used in PDR models (e.g., Tielens & Hollenbach 1985). We estimate that the absolute value of G_0 derived here may have a systematic uncertainty of 50%, taking account of the uncertainty in the absolute calibration of the LWS and the contribution from low-energy photons, but that the relative value is accurate within 30%.

3. Results

3.1. Intensity distribution

The line intensities, *FIR*, and G_0 are listed in Tables 2 and 3, where the intensities larger than 2σ are listed with the errors (1σ) in the parentheses. The errors of the line intensities come mostly from the uncertainty in the baseline estimate and do not include the uncertainty in the absolute calibration (~50% for extended sources, Gry et al. 2002). At the position near η Car ((l, b) = (287.°61, −0.°64)) the continuum is steeper than the graybody with the emissivity of the power law index of unity because the emission from η Car has a large contribution to the observed spectrum. Therefore *FIR* and G_0 are not derived at this position. The intensity maps of [O I] 63 μm, 145 μm, [C II] 158 μm, and [N II] 122 μm are shown in Fig. 3, while those of [Si II] 35 μm and H_2 9.66 μm are shown in Fig. 4. The maps of *FIR* and G_0 are shown in Fig. 5. Paper I shows that highly-ionized ionic lines, [O III] 52 μm, 88 μm, and [N III] 57 μm, are detected in the entire observed region and that the three ionic line emissions have spatial distributions similar to each other, which peak around Car I. The [O I] 63 μm, [N II] 122 μm, [C II] 158 μm, and [Si II] 35 μm emissions are detected at all the observed positions, indicating that these species are also distributed widely in the observed region, but their spatial distributions are different from the highly-ionized gas emissions.

The [O I] 63 μm peak is located at (l, b) = (287.°36, −0.°69), the edge of the molecular cloud facing to the Car I OB star cluster. Strong [O I] 63 μm emission was detected also at the position north-west next to η Car and the positions 0.°1 north to Car I. The [O I] 145 μm emission was much weaker than the 63 μm emission and detected only at 10 positions in marginal levels (~(2.5−3)σ). For these positions the average ratio of [O I] 145 μm to 63 μm is 0.09 ± 0.01 except for the position of (l, b) = (287.°41, −0.°54), where the ratio is 0.04 and the contribution from shocked gas is suggested to be significant (see below). While the derived intensity of [O I] 145 μm should be examined with care because of the marginal detection, the ratio of [O I] 145 μm to 63 μm at the 9 positions are in agreement with each other, suggesting that the average ratio indicates a representative value for these positions, particularly in the interface region ((l, b) = (287.°41, −0.°64), (287.°41, −0.°69), (287.°46, −0.°69), and (287.°36, −0.°69)). The detection limit is

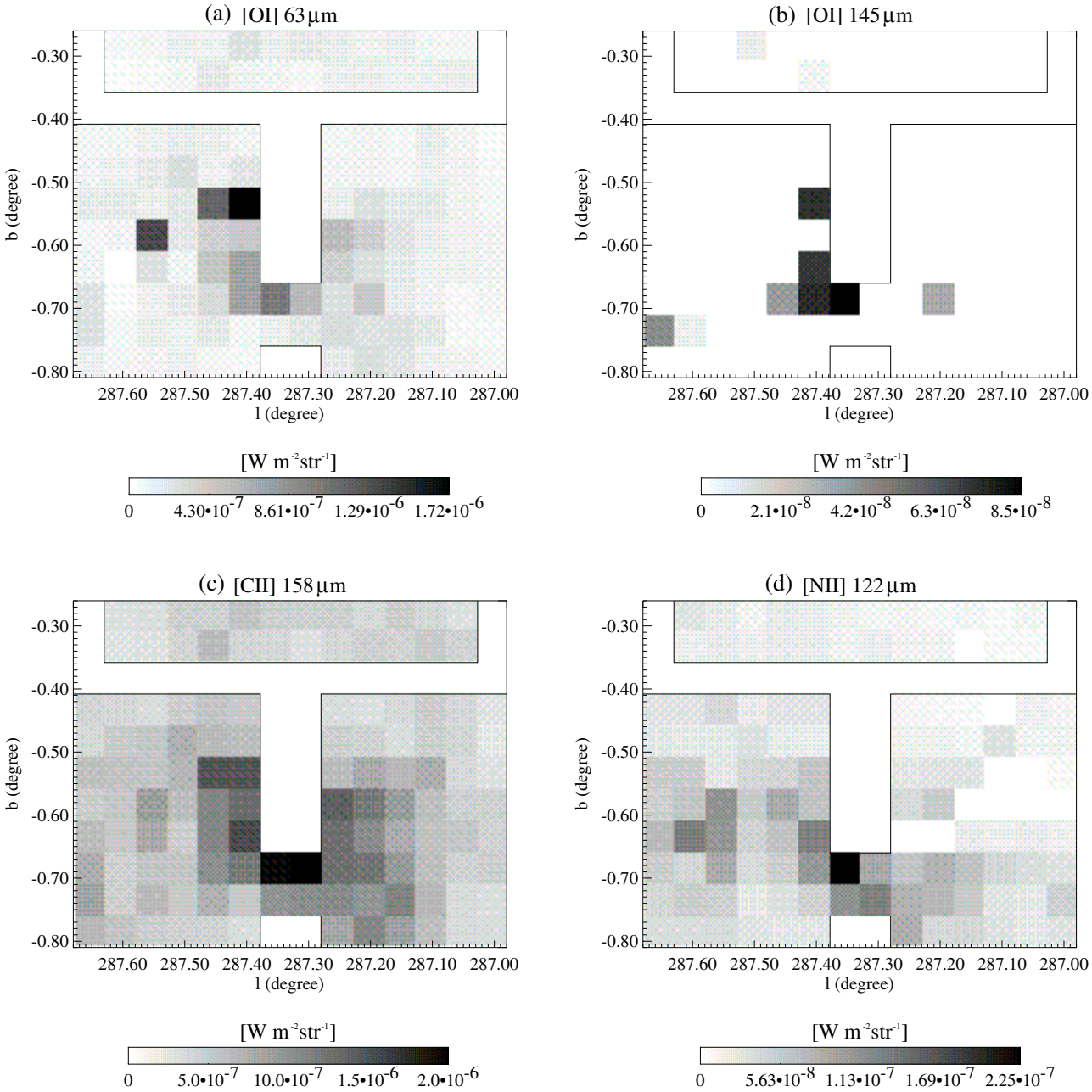

Fig. 3. Intensity maps of the emission lines plotted in the Galactic coordinates: **a)** [O I] 63 μm, **b)** [O I] 145 μm, **c)** [C II] 158 μm, and **d)** [N II] 122 μm. The observations were not executed for the T-shaped area enclosed by the solid lines. In the observed area, white color grid indicates the positions where the line intensities are smaller than 2σ uncertainties.

approximately 1.0×10^{-8} W m^{-2} sr^{-1} and 2.0×10^{-9} W m^{-2} sr^{-1} for the 63 μm and 145 μm lines, respectively.

The [N II] emission peaks at the position near the east side of the border region between the H II region and molecular cloud. The emission seems to be slightly shifted to east or to the ionized side of the PDR compared to the distribution of the [O I] 63 μm emission.

The [C II] emission peaks at the center of the observed area, around the interface region between the H II region and the molecular cloud. Diffuse [C II] emission was detected even in the direction of the dark lane or the surrounding region, which is far from the optically-bright area, suggesting a large contribution from the diffuse component. The intensity is quite strong and ranges from 1.0×10^{-7} to 1.2×10^{-6} W m^{-2} sr^{-1}.

The [Si II] 35 μm emission peak is located near the interface region, but it is slightly shifted to the H II region. The emission can roughly be divided into two components: one is the component peaking around the Tr 14 cluster, and the other is the diffuse emission detected in the whole observed area. The intensity increases steeply toward the peak and the peak intensity is higher than that of the [C II] emission. The [Si II] intensity in the outer region is about the same as the [C II] emission. In addition, strong [Si II] emission is seen at the position closest

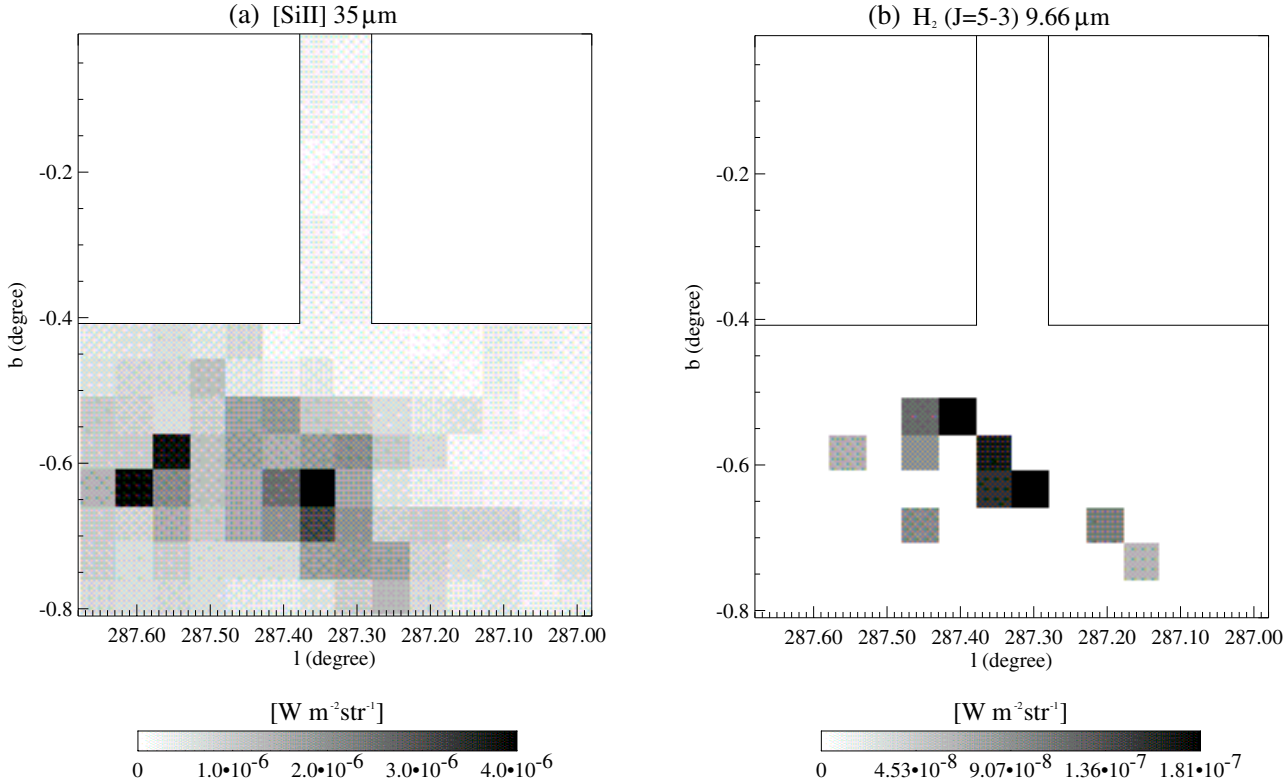

Fig. 4. Intensity maps of [Si II] 35 μm line **a)** and H_2 9.66 μm rotational line **b)**. The white color grid in **b)** indicates the positions where the line intensities are smaller than 2σ uncertainties.

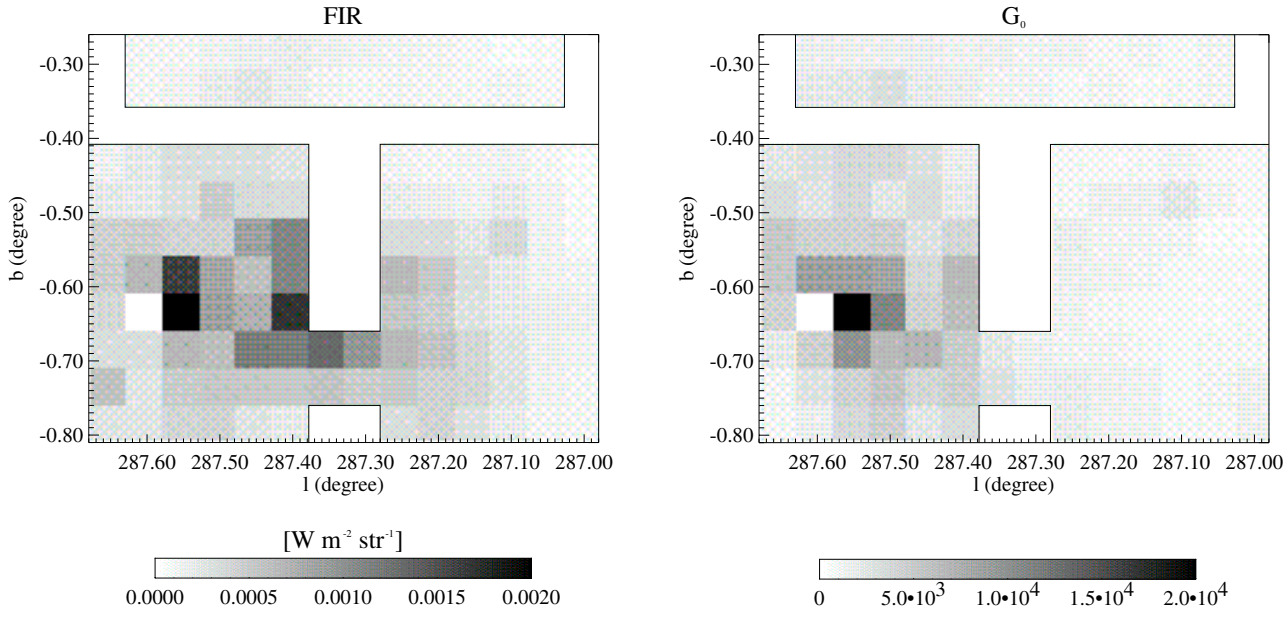

Fig. 5. Maps of the total FIR intensity FIR **a)** and the radiation field strength G_0 in units of 1.6×10^{-6} Wm^{-2} **b)**. The notations are the same as in Fig. 3.

to η Car and north-west to η Car ((l, b) = (287.°61, −0.°64) and (287.°56, −0.°59)).

The pure rotational transition of H_2 (J = 5–3) at 9.66 μm is much weaker than the other lines and detected only in the central region of the observed area and near η Car. The emission requires high densities and high temperatures and is supposed to come mainly from the interface region. Strong emission was detected at (l, b) = (287.°41, −0.°54), (287.°46, −0.°54), and (287.°56, −0.°59) towards the regions of strong [O I] 63 μm emission.

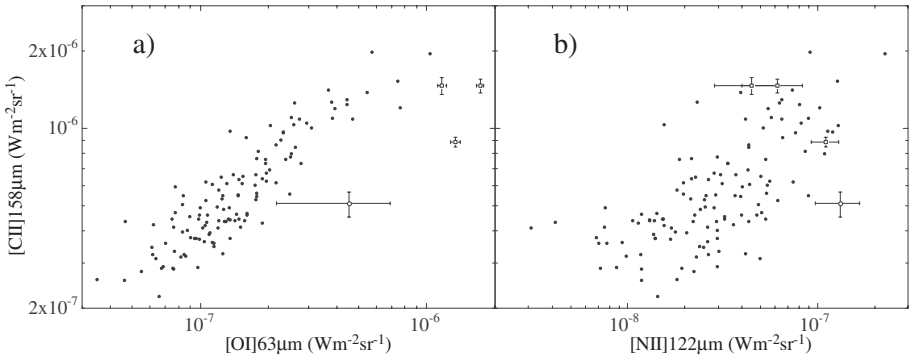

Fig. 6. Correlation of [C II] 158 μm with **a)** [O I] 63 μm and **b)** [N II] 122 μm. The open circle shows the data toward η Car and the open squares indicate those of high density regions (see text). The error bars for the filled circles are listed in Table 2 and not shown here.

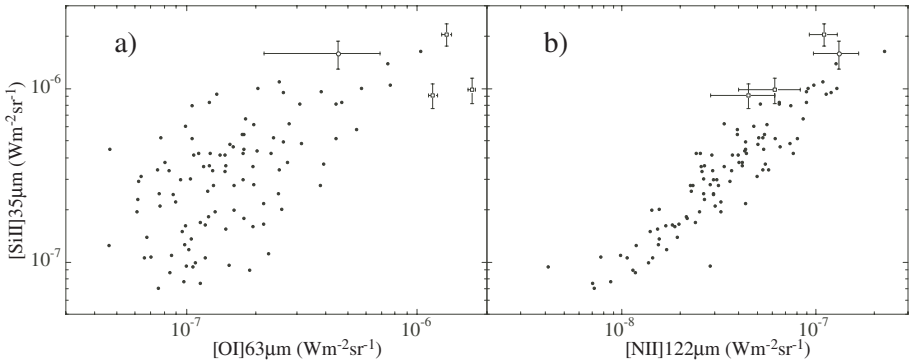

Fig. 7. Correlation of [Si II] 35 μm with **a)** [O I] 63 μm and **b)** [N II] 122 μm. The symbols are the same as in Fig. 6.

3.2. Intensity correlation

Because the first ionization energy of oxygen is slightly larger than hydrogen, the [O I] lines are thought to originate mainly from the neutral gas or PDRs, whereas the [N II] 122 μm line comes mostly from the diffuse ionized gas because of its low critical density for the collisional excitation by electrons. The [C II] 158 μm and [Si II] 35 μm lines, on the other hand, can originate from both the neutral and ionized gas. In the following, we simply assume that [O I] 63 μm represents the PDR component and [N II] 122 μm traces the lowly-ionized diffuse gas. The origin of the [C II] 158 μm and [Si II] 35 μm emissions is investigated based on the correlation with these two lines.

Figure 6 plots the [C II] 158 μm intensity against the [O I] 63 μm and [N II] 122 μm intensities. The [C II] 158 μm and [O I] 63 μm emissions show a good linear correlation with each other (the correlation coefficient of 0.90) in the observed area for $I([\mathrm{O\,I}]\,63\,\mu\mathrm{m}) \leq 4.0 \times 10^{-7}$ W m^{-2} sr^{-1}, suggesting that the [C II] 158 μm emission is mainly associated with the PDR. At the positions with the strong [O I] 63 μm emission, the [C II] intensity does not increase with the [O I] intensity. These positions correspond to the directions toward η Car, north-west next to η Car, (287.°41, −0.°54), and (287.°46, −0.°54). The large difference in the critical densities between these two transitions leads to the saturation in the [C II] 158 μm intensity relative to [O I] 63 μm at the high density regime ($10^5 < n < 10^7$ cm^{-3}). It is likely that the peculiar star, η Car, compresses the surrounding medium by its stellar wind or radiation pressure and produces a high-density shocked gas around it, although the high density matter in the surroundings of η Car is rather scarce (Cox 1995; Cox & Bronfman 1995). While we have no particular information on the other two positions, the detection of strong [Si II] emission and H_2 emission at the same positions supports the presence of high-density gas in these directions. The [C II] 158 μm and [N II] 122 μm emissions show a weak correlation (the correlation coefficient of 0.25; Fig. 6b). The contribution from the ionized gas to the [C II] emission is thus suggested to be less significant than that from the neutral gas. The offset component seen in the [O I] 63 μm and [C II] 158 μm correlation (Fig. 6a) can be attributed to the emission from the diffuse ionized gas.

In the following analysis we assume that the contributions to the [C II] 158 μm emission from the PDR and ionized gas are simply proportional to the intensity of [O I] 63 μm and [N II] 122 μm, respectively, for $I([\mathrm{O\,I}]\,63\,\mu\mathrm{m}) < 4 \times 10^{-7}$ W m^{-2} sr^{-1}, which excludes the shocked regions.

By a least-squares fit we obtain

$$I([\mathrm{C\,II}]\,158\,\mu\mathrm{m}) = (2.82 \pm 0.03) \times I([\mathrm{O\,I}]\,63\,\mu\mathrm{m}) + (3.74 \pm 0.10) \times I([\mathrm{N\,II}]\,122\,\mu\mathrm{m}). \quad (3)$$

The derived intensity ratio of [C II] 158 μm to [O I] 63 μm of 2.82 in the PDR indicates that the [C II] 158 μm is the dominant cooling line in the Carina nebula region. The average fraction of the contribution to [C II] 158 μm from the PDR in the Carina nebula is estimated by subtracting the contribution from the ionized gas estimated as $3.74 \times I([\mathrm{N\,II}]\,122\,\mu\mathrm{m})$ at each position and found to be about 80 ± 10%.

Figure 7 plots the correlations of [Si II] 35 μm with [O I] 63 μm and [N II] 122 μm. The effect of extinction is estimated from the COBE data and CO observations and found to be insignificant at 35 μm ($\tau_{35\ \mu\mathrm{m}} < 0.3$) except for a few positions in the molecular cloud region (Paper I). The [Si II] 35 μm emission shows a good correlation with [N II] 122 μm in the whole observed area (the correlation coefficient of 0.89), whereas the correlation with [O I] 63 μm is very weak (the correlation coefficient of 0.04). It is thus suggested that the

[Si II] 35 μm emission originates mostly from the ionized gas and that the contribution from the PDR is not significant. A least-squares fit gives

$$I([\mathrm{Si\,II}]\,35\,\mu\mathrm{m}) = (0.30 \pm 0.01) \times I([\mathrm{O\,I}]\,63\,\mu\mathrm{m}) + (7.94 \pm 0.05) \times I([\mathrm{N\,II}]\,122\,\mu\mathrm{m}). \quad (4)$$

The correlation study must take account of the effect of the difference in the beam sizes between [Si II] 35 μm ($20'' \times 33''$), and [O I] 63 μm and [N II] 122 μm ($\sim 80''$). Because of the small beam size [Si II] 35 μm may be affected by local fluctuations most severely. The good correlation between [Si II] 35 μm and [N II] 122 μm, however, suggests that both emissions are dominated by the smooth diffuse component and that local fluctuations do not affect the correlation significantly, if any. Since we have derived the slope constant of 7.9 based on 100 data points with a small uncertainty, this number should represent the true ratio fairly well.

4. Discussion

4.1. Origin of C II emission

The present observations suggest that a large fraction of the [C II] 158 μm emission comes from the PDR and indicate the presence of neutral gas in whole the observed region. The diffuse [C II] 158 μm emission in the Galactic plane has been detected in several observations (e.g. Shibai et al. 1991, 1996; Wright et al. 1991; Makiuti et al. 1996, 2002; Nakagawa et al. 1998). Shibai et al. (1991) suggested that the diffuse [C II] emission originates mostly from diffuse PDRs, while Heiles (1994) pointed out the extended low density warm ionized medium as an alternative source for the emission. The present results suggest that a large fraction ($\sim$80%) of the diffuse [C II] emission in the active star-forming region of the Carina nebula comes from the diffuse PDR associated with the [O I] 63 μm emission, supporting the suggestion by Shibai et al. (1991).

The contribution from the ionized gas to the [C II] 158 μm emission can be estimated from Eq. (3) as $3.74 \times I([\mathrm{N\,II}]\,122\,\mu\mathrm{m})$. We estimate the electron density by simply assuming that the derived coefficient indicates a mean ratio in the diffuse ionized gas. The correlation is weak and thus this gives only a crude estimate. The present ratio is compatible with the mean ratios reported for external galaxies ($\sim$3.5, Negishi et al. 2001; $\sim$4.3, Malhotra et al. 2001). The expected line intensity ratio for the optically thin case in the ionized gas is given by

$$\frac{I_{158\,\mu\mathrm{m}}}{I_{122\,\mu\mathrm{m}}} = \frac{A_{158\,\mu\mathrm{m}}}{A_{122\,\mu\mathrm{m}}} \times \frac{n(\mathrm{C\,II})f(\mathrm{C\,II})}{n(\mathrm{N\,II})f(\mathrm{N\,II})}, \quad (5)$$

where A, n, and f are the Einstein coefficient, the density, and the fraction of the excited populations of C^+ and N^+. The ratio of $A_{158\,\mu\mathrm{m}}/A_{122\,\mu\mathrm{m}}$ is 0.25 according to Nussbaumer & Storey (1981) and Mendoza (1983). We assume the interstellar gas phase abundance for C and N, such that the abundances of C and N relative to that of hydrogen are 1.4×10^{-4} and 7.9×10^{-5}, respectively (Savage & Sembach 1996). Both C and N are assumed to be all in the singly ionized state. The line ratio is almost independent of the gas temperature higher than 5000 K and we assume the temperature to be 8000 K in the estimate. Then the ratio of 3.74 indicates an electron density of about 10 cm^{-3}. If we assume the latest solar abundance without depletion for C and N (C = 3.9×10^{-4} H and N = 8.5×10^{-5} H; Holweger 2001), the electron density will be about 50 cm^{-3}. The electron density of the [N II] 122 μm emitting gas in the Galactic plane has been estimated to be less than 100 cm^{-3} and typically 10–30 cm^{-3} by COBE observations (Wright et al. 1991), which is in agreement with the present estimate. In Paper I we estimate the electron density of the diffuse extended component of the [O III] 52, 88 μm and [N III] 57 μm emitting gas as less than 100 cm^{-3} in the Carina nebula region. Compared to this value the suggested electron density for the [N II] emitting gas is in a similar or slightly smaller range.

The [N II] 122 μm emission has been detected at each position where [N III] 57 μm has been detected, indicating the presence of gases with different ionization states in the same line of sight. The extended [N III] 57 μm emission is suggested to come from very thin sheets in addition to the diffuse component (Paper I). The [N II] 122 μm is supposed to originate from the diffuse ionized gas surrounding the N^{++} thin sheets. Sembach et al. (2000) have shown that singly ionized N^+ and C^+ are the dominant ionization states in the diffuse ionized gas: 81% of N is in N^+ and 95% of C is in C^+. Taking account of the different ionization states, the true N^+ abundance relative to C^+ should be reduced only by 15% and we can conservatively estimate an upper limit of the diffuse ionized gas density to be 100 cm^{-3}.

4.2. Physical conditions of the PDR

The intensity ratio of the correlated component of [C II] 158 μm to [O I] 63 μm is large ($\sim$2.8) and constant over the observed region. It does not show any systematic trend with the distribution of the ionized gas or the molecular gas. The contribution from the ionized gas is in a reasonable range as discussed above. It is well constrained by the [N II] 122 μm intensity and could not be appreciably larger than the presently estimated value, which indirectly supports the attribution of the [C II] component correlated with [O I] 63 μm to the PDR origin. Thus the large constant ratio in the PDR is not a spurious result from the correlation analysis and should be interpreted in terms of physical models. The observed region is supposed to have appreciable variations in the physical conditions, such as temperature and density. The observed constancy of the intensity ratio indicates either that the physical conditions of the line-emitting gas do not change largely and/or that there are some mechanisms to maintain the intensity ratio constant.

Simple model calculations of optically-thin collisionally-excited isothermal neutral gas show that the line intensity ratio of [C II] 158 μm to [O I] 63 μm emissions is sensitive to the gas density for $n > 1 \times 10^3$ cm^{-3} (Watson 1984). The ratio becomes independent of n and depends only on the temperature for $n < 1 \times 10^3$ cm^{-3}, which is well below the critical densities of both transitions. The observed ratio of about 2.8 can be obtained for $300 < T < 500$ K and $n < 1 \times 10^3$ cm^{-3} in the simple model. For higher densities [O I] 63 μm emission becomes stronger and the ratio decreases. The gas abundance

of oxygen and carbon is suggested to be rather constant in a wide range of the physical conditions and the depletion factor of both elements is only about −0.4 (Cardelli et al. 1996; Savage & Sembach 1996; Sofia et al. 1997; Cartledge et al. 2001). Thus the uncertainty in the abundance should not affect the results largely.

The intensity ratio of the [O I] 145 μm to 63 μm emissions is an indicator of the temperature of the gas in the low density regime ($n < 10^5$ cm^{-3}) because both lines have large critical densities (>10^6 cm^{-3}) and the 145 μm line requires high temperatures to be excited (327 K). The average ratio of the [O I] 145 μm to 63 μm at 9 positions where the [O I] 145 μm emission is marginally detected is 0.09 ± 0.01. Model calculations of optically-thin collisionally-excited neutral gas show that the intensity ratio can reach the observed average value of 0.09 only when $T > 1000$ K and $n < 10^3$ cm^{-3}. Below 1000 K the intensity ratio becomes much lower than 0.09. Since the average ratio of [C II] 158 μm to [O I] 63 μm for the regions with the detected [O I] 145 μm is also 2.7, the simple model cannot account for the observed intensities of the [O I] 63 μm, 145 μm, and [C II] 158 μm emissions consistently.

Indirect excitation of the $^3P_1$ and $^3P_0$ levels in O I can result by cascades from higher states that have been populated from $^3P_2$ through absorption of the ultraviolet (UV) radiation and this UV pumping can enhance the [O I] 145 μm emission (Keenan et al. 1994). The UV pumping can make the [O I] 145 μm to 63 μm ratio as large as 0.7 at low densities (e.g. $n < 1000\,$cm^{-3} and $T < 1000\,$K, Okada et al. 2003). However this mechanism should be most effective in the vicinity of the heating source. In the present observations [O I] 145 μm is detected only near the interface between the ionized gas and molecular cloud, suggesting that the UV pumping is not a major mechanism for the observed large ratio of [O I] 145 μm to 63 μm.

In a wide parameter range of PDRs the optical depth of the [O I] 63 μm transition exceeds unity and the line intensity becomes small compared to optically-thin calculations (e.g., Kaufman et al. 1999). In the following we examine the observations in the framework of PDR models that take account of the radiative transfer effect as well as the chemistry and energy balance of the gas.

The photoelectric heating is thought to be the dominant heating mechanism in PDRs (de Jong et al. 1980). In this process ultraviolet photons are absorbed by dust grains and photoelectrons are ejected from the grains. The excess energy of the ejected electrons over the work function is then distributed to the neutral gas. The gas is collisionally heated by hydrogen atoms and cooled by far-infrared line emissions. The strength of the incident radiation G_0 and the density of the gas n are the two major parameters in the model calculations. In the PDR [O I] 63 μm and [C II] 158 μm are dominant cooling lines and the ratio of ([C II] 158 μm + [O I] 63 μm)/FIR provides an observational measure for the efficiency of the photoelectric heating. We estimate the ratios by subtracting the contribution from the ionized gas to [C II] 158 μm and plot them against G_0 in Fig. 8. The ratio ranges from 0.0006 to 0.012, being compatible with the range suggested by previous

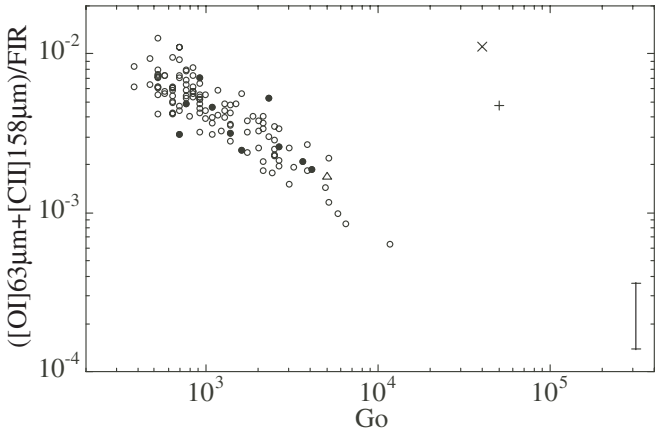

Fig. 8. Photoelectric heating efficiency ([O I] 63 μm + [C II] 158 μm)/*FIR* versus G_0. The filled circles indicate the data of the positions where [C II] 145 μm was detected and the open circles those without detection. The ratios in other objects are indicated by different symbols: W49N (bar, Vastel et al. 2001), M17SW (plus, Meixner et al. 1992), Orion bar (cross, Tauber et al. 1994), and 30 Doradus (open triangle, Stacey et al. 1991; Poglitsch et al. 1995).

observations (e.g., Stacey et al. 1991). It decreases with G_0 approximately as $\propto 1/G_0$. According to PDR models (Wolfire et al. 1990; Kaufman et al. 1999) the ratio is roughly a function of G_0/n and varies as $(G_0/n)^{-\alpha}$ ($0.5 < \alpha < 1$) for the range of $10^2 < G_0 < 10^4$ and $10^2 < n < 10^4\,$cm^{-3}. Thus it is suggested that the gas density decreases slightly with G_0 in the observed region. Brooks et al. (2003) have derived the efficiency of 5×10^{-3} and $G_0 = 10^3$–10^4 for Tr 14, which are compatible with the present results.

In Fig. 8 also plotted are the photoelectric heating efficiencies of other PDRs associated with H II regions (Vastel et al. 2001, and references therein). PDRs in 30 Doradus and W49 have densities of 3×10^3–1×10^4 and $\sim 10^4\,$cm^{-3}, respectively (Vastel et al. 2001; Poglitsch et al. 1995), which are similar to or slightly larger than those derived for the Carina PDRs. The photoelectric heating efficiency of 30 Doradus (open triangle) is well on the trend of the Carina data and that of W49 (bar) seems to be on the line extrapolated from the trend. The photoelectric heating efficiencies of M17SW (plus) and the Orion bar (cross) are located above the present trend. The suggested clump densities of these regions are much higher than the Carina region (5×10^5 and $10^6\,$cm^{-3}, respectively, Meixner et al. 1992; Tauber et al. 1994). Taking account of the suggested densities, these data can be interpreted consistently in terms of the dependence of the photoelectric heating efficiency on (G_0/n). Therefore they suggest that the variations in the photoelectric heating efficiency derived in various PDRs are in agreement with the model prediction and the trend seen in the Carina PDRs suggests that the gas density decreases slightly with G_0 in the observed area.

First we compare the observations with the model by Wolfire et al. (1990), which predicts the line ratio of [C II] 158 μm to [O I] 63 μm to be around 3 for $500 < G_0 < 5000$ and $1000 < n < 3000\,$cm^{-3}. Since G_0 varies at least by a factor of 10 over the observed area, the observed constancy

requires some correlation between G_0 and n, such that n decreases as G_0 increases. It is qualitatively in agreement with the trend suggested by ([O I] 63 μm + [C II] 158 μm)/FIR with G_0 and is compatible with the fact that the high-density molecular gas is located away from the exciting stars. In the same parameter range, however, the predicted ratio of [O I] 145 μm to 63 μm is about 0.04. This is far below the observed ratio of 0.09 ± 0.01. Thus the present observations cannot be interpreted solely in terms of the model of Wolfire et al. (1990).

Kaufman et al. (1999) employ the most recent physical constants and take account of the contribution from polycyclic aromatic hydrocarbon (PAH) molecules to the photoelectric heating. The heating through PAHs increases the gas temperature significantly compared to previous models and enables to produce the intense [O I] 145 μm line emission. In the parameter range of $500 < G_0 < 5000$ and $n < 1000\,\mathrm{cm}^{-3}$, the model predicts the ratio to be 0.07–0.08, which is marginally compatible with the observed ratio of 0.09 ± 0.01. However the model also predicts the ratio of [C II] 158 μm to [O I] 63 μm to be around unity, much smaller than the observed value of 2.8, for the same parameter range. The model cannot produce the ratio of 2.8 for $G_0 > 100$. Even in the low-density limit with the interstellar abundance, the contribution to [C II] 158 μm from the ionized gas estimated from [N II] 122 μm cannot exceed 30% of the observed [C II] intensity and the ratio of [C II] 158 μm to [O I] 63 μm in the PDR should not be smaller than 2. Thus, in the range of G_0 suggested by the *FIR* color as well as the stellar distribution in the region, the model of Kaufman et al. (1999) cannot account for the large [C II] 158 μm to [O I] 63 μm ratio. The small [C II] 158 μm to [O I] 63 μm ratio of the model results from the high heating efficiency owing to PAHs. The photoelectric heating will be reduced if PAHs are positively charged because of the increase of the electrostatic potential. While the ubiquitous presence of PAHs in the Carina nebula has been suggested by observations of the 3.3 μm band (Rathborne et al. 2002), Chan et al. (2001) have indicated that most interstellar PAHs, particularly in the Carina nebula, are positively charged and the photoelectric heating through PAHs should be suppressed. Then the [O I] 63 μm emission can be weaker than the prediction. However in this case the observed large ratio of [O I] 145 μm to 63 μm cannot be accounted for because the [O I] 145 μm transition has a higher excitation energy than the 63 μm transition and thus [O I] 145 μm should be more significantly reduced. Liseau et al. (1999) have examined the collision coefficients of the [O I] transitions in detail, but model calculations with the new collision parameters did not show a significant difference. Thus the uncertainty in the collision parameters is not a major factor for the discrepancy among the observed line intensities of [O I] 63 μm, 145 μm, and [C II] 158 μm.

Large ratios of [O I] 145 μm to 63 μm have been reported also in other objects (Liseau et al. 1999; Caux et al. 1999; Giannini et al. 2000; Okada et al. 2003) and it has been suggested that absorption by cold foreground oxygen atoms makes a significant effect on the ratio. The optical depth of [O I] 63 μm becomes unity for $N_{\mathrm{H}} = 1 \times 10^{21}$ cm^{-2} (Tielens & Hollenbach 1985). ^{12}CO observations (Brooks et al. 1998) of the Carina nebula suggest that $N_{\mathrm{H}} = (1\text{–}6) \times 10^{22}$ cm^{-2} in the directions where [O I] 145 μm is detected. Therefore, even if only a few percent of O I indicated by the CO intensity intersects the line of sight between the PDR region and us, a large fraction of the [O I] 63 μm emission could be attenuated relative to [C II] 158 μm and [O I] 145 μm by the foreground cloud, where carbon should be mostly in CO and no significant absorption of [C II] 158 μm is expected. Absorption of [O I] 63 μm also affects the ratio of [C II] 158 μm to [O I] 63 μm. If we take $n = 10^3$ cm^{-3} and $G_0 = 10^3$ as typical parameters for the interface region of the Carina nebula, the PDR model of Kaufman et al. (1999) predicts the ratios of [C II] 158 μm/[O I] 63 μm and [O I] 145 μm/63 μm to be about 0.7 and 0.07, respectively. The difference between the observation and the model is about a factor of 4 for [C II] 158 μm/[O I] 63 μm, while it is only 20% for [O I] 145 μm/63 μm. In the parameter range of $500 < G_0 < 5000$ and $100 < n < 1000\,\mathrm{cm}^{-3}$ the trend of discrepancy remains unchanged. Thus the foreground absorption of [O I] 63 μm cannot resolve the discrepancy with the present observations even if all the possible errors are taken into account. Furthermore the [C II] 158 μm/[O I] 63 μm ratio is fairly constant over the observed area. Therefore if the large ratio is attributed to the foreground absorption of [O I] 63 μm, it requires uniform absorption over the entire observed area, which seems very unlikely. We conclude that the model with the efficient PAH heating of Kaufman et al. (1999) cannot account for the present observations consistently even if absorption of [O I] 63 μm is taken into account.

Recently, Okada et al. (2003) have suggested that [C II] 158 μm could also be absorbed to some extent together with [O I] 63 μm if several PDRs overlap on the line of sight or if we look at the PDR nearly in the edge-on view because the optical depth of the [C II] 158 μm line is about unity in PDRs. The fraction of the absorbed [C II] 158 μm emission depends on the overlapping degree, and is typically about 60% of that of [O I] 63 μm. This mechanism leads to an increase in the [O I] 145 μm to 63 μm ratio, but the ratio of [C II] 158 μm to [O I] 63 μm is only slightly affected. Thus if the intrinsic line intensities are those predicted by Wolfire et al. models or the efficient heating via PAHs is suppressed due to the charge-up effect, then the present observations may be accounted for by the overlapping PDR model. Absorption features of the [C II] 158 μm and [O I] 63 μm lines have been detected in several objects with high spectral-resolution observations (Boreiko & Betz 1995, 1997; Poglitsch et al. 1996; Kraemer et al. 1998; Baluteau et al. 1997; Vastel et al. 2000). Detailed modeling and high spectral-resolution observations would be quite interesting to examine the significance of the absorption of these two lines in the Carina nebula region.

4.3. Silicon abundance in diffuse ionized gas

As discussed in Sect. 4.1, the present observations indicate the presence of gases with different ionization states in the same line of sight in the Carina nebula. Sembach et al. (2000) have shown that singly ionized N^+ and Si^+ are the dominant ionization states in the diffuse ionized gas: 81% of N is in N^+ and 91% of Si in Si^+. Both [N II] 122 μm and [Si II] 35 μm

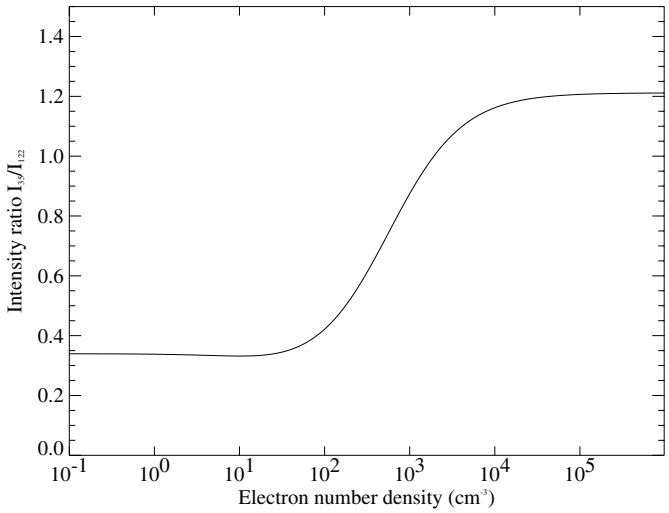

Fig. 9. Expected intensity ratio of [Si II] 35 μm to [N II] 122 μm for T_e = 8000 K with the interstellar abundance of Si and N (see text).

emissions originate mostly from the diffuse ionized component. Therefore both [N II] 122 μm and [Si II] 35 μm can be assumed to come from the same ionized gas as suggested by the good correlation despite of the large difference in the ionization energy.

Figure 9 shows the [Si II] 35 μm/[N II] 122 μm intensity ratio calculated for the ionized gas, assuming that their elemental depletions relative to the solar abundance are 0.025 for Si and 1.0 for N (Tielens & Hollenbach 1985) or the gas phase abundance of Si and N is assumed to be 3.4×10^{-5} H and 8.5×10^{-5} H, respectively. The collision strength for the [Si II] 35 μm is taken from Osterbrock (1989). The observed ratio is about 7.9, far above the predicted value in Fig. 9. If we assume the electron density of less than 100 cm^{-3} as indicated by the [C II] 158 μm to [N II] 122 μm ratio from the ionized gas, the required gas phase silicon abundance must be by 22 times larger. Taking account of the 10% difference in the ionization fraction, the observed ratio of [Si II] 35 μm/[N II] 122 μm indicates that Si of about half of the solar abundance must be in the gas phase relative to N. The present results suggest that a significant fraction of Si returns from dust grains to the gas phase in the diffuse ionized gas.

As discussed in Sect. 3.2, the good correlation suggests that local fluctuations of [Si II] 35 μm, if any, should not be significant and the difference in the beam sizes between [Si II] 35 μm and [N II] 122 μm does not affect the results significantly. Large uncertainties in the beam pattern of the LWS (Gry et al. 2002) may result in systematic errors in the relative band intensity. However, even if we take into account the errors in the absolute calibration of the LWS (~50%), [Si II] 35 μm is still very strong relative to [N II] 122 μm and the conclusion that a large fraction of Si (>25% of solar) must reside in the gas phase is not altered.

The [Si II] 35 μm emission can also originate from PDRs. Because of the high critical density for the collision with hydrogen atoms and the high excitation energy, however, [Si II] 35 μm requires high-density and high-temperature gas to be excited efficiently (see Table 1). With the parameter range derived in the previous subsection ($n < 3000$ cm^{-3}), the [Si II] 35 μm emission from PDRs cannot be significant. Based on the low-density PDR model by Hollenbach et al. (1991), the [Si II] 35 μm emission has a dependence on the density similar to [O I] 63 μm. The observed [Si II] 35 μm emission is as strong as [O I] 63 μm (see Fig. 7), which can be accounted for only by nearly solar abundance Si gas in the PDR for densities less than 10^5 cm^{-3}. Supported by the good correlation with [N II] 122 μm we conclude that the contribution from PDRs to [Si II] 35 μm in the Carina region is insignificant. Even if we take account of a possible contribution from PDRs, a large Si abundance in the gas phase is a secure conclusion.

Strong [Si II] 35 μm emission has been detected in several objects. Based on the spatial distribution and the line profile of [Si II] 35 μm, Stolovy et al. (1995) have suggested dust destruction via cloud-cloud collisions in the Galactic center region. With FIR spectroscopic observations, Carral et al. (1994) have indicated that Si gas of half the solar abundance must be in H II regions of the starburst galaxy NGC 253, while 25% solar abundance of Si is suggested to be in the ionized gas in the Sharpless 171 region (Okada et al. 2003). The present value of the gas phase Si abundance is compatible with the result of NGC 253, suggesting that the Carina nebula region has harsh environments similar to starburst galaxies.

Theoretical investigations have shown that dust grains are destroyed quite efficiently by supernova shocks in a time scale of $(2-4) \times 10^8$ yr (Jones et al. 1994, 1996). The supply of dust grains from stellar sources has a much longer time scale and cannot balance with the destruction by supernova shocks in the ISM (Draine 1990). Thus most interstellar grains are thought to be formed in interstellar clouds and recycling of dust grains should take place in a short time scale (Dwek 1998). Seab & Shull (1983) indicated a variation in the UV extinction curve, which can be attributed to the shock processing. The Goddard High Resolution Spectrograph (GHRS) on board the Hubble Space Telescope has provided a large amount of new data of the elemental gas abundance in interstellar space (Savage & Sembach 1996, and references therein). These observational results indicate that Si returns to the gas phase relatively quickly while Fe seems to be more resistive (Fitzpatrick 1996, 1997). The present observations provide direct evidence that destruction of Si-bearing grains can occur efficiently in active star-forming regions like the Carina nebula. These results together with the constant gas phase abundance of oxygen and carbon (Cardelli et al. 1996; Sofia et al. 1997; Cartledge et al. 2001) give a new insight into the dust destruction process in the ISM. The recycling as well as the composition of dust grains in the interstellar space must be reexamined based on these latest results of the interstellar abundance (cf., Tielens 1998; Jones 2000; Onaka 2000).

5. Summary

We have presented mapping results of the H II region and molecular cloud complex of the Carina nebula based on spectroscopic results obtained using the SWS and LWS instruments on board ISO. The line emissions of [O I] 63 μm, 145 μm, [C II] 158 μm, [N II] 122 μm, [Si II] 35 μm, and H_2 9.66 μm are

investigated in the present paper. Strong emissions of these lines are observed in the direction to the border region between the H II region and molecular cloud. In addition, [O I] 63 μm, [C II] 158 μm, [N II] 122 μm, and [Si II] 35 μm have been widely detected in the surrounding region. H_2 9.66 μm is detected only at 7 positions and [O I] 145 μm, is marginally detected at 10 positionss.

The correlation between the [O I] 63 μm and [C II] 158 μm intensities indicates that [C II] 158 μm emission mainly comes from the PDR and a correlation between the gas density and the radiation field strength is suggested. The [C II] 158 μm to [O I] 63 μm ratio is large (~2.8), indicating a low gas density ($n \leq 3 \times 10^3$ cm^{-3}) and a low gas temperature, while the large [O I] 145 to 63 μm ratio indicates a high temperature. For the positions where [O I] 145 μm emission has been marginally detected, the [O I] 63 μm, 145 μm and [C II] 158 μm line intensities cannot be accounted for consistently by the latest PDR model with the efficient photoelectric heating via PAHs even if absorption of [O I] 63 μm by foreground cold gas is taken into account. Absorption of [C II] 158 μm together with [O I] 63 μm by overlapping PDRs, in which the heating via PAHs is suppressed, may account for the observed intensities of the [O I] 63 μm, 145 μm, and [C II] 158 μm emissions at these positions.

The good correlation with [N II] 122 μm suggests that the [Si II] 35 μm emission in the Carina nebula comes mostly from the ionized gas. The intensity ratio of [Si II] 35 μm to [N II] 122 μm indicates that in the Carina nebula Si should be in the gas phase with an abundance of about half solar, suggesting that a large fraction of Si in dust grains should be brought back to the gas phase and that efficient dust destruction is occurring. The present results indicate the importance of observations of [Si II] 35 μm in the future to study the dust processing in the ISM.

Acknowledgements. We would like to thank the referee Pierre Cox for his many useful comments and suggestions that improved the paper. We would like to thank S. Sidher and the LWS IDT in Rutherford Appleton Laboratory for their help in the LWS data processing, and I. Yamamura and the SWS Instrument Dedicated Team (IDT) for their help in the SWS data reduction. We also wish to thank K. Kawara, Y. Satoh, H. Okuda, and the Japanese ISO team for their continuous help and encouragement. This work was supported in part by Grant-in-Aids for Scientific Research from Japanese Society for the Promotion of Science.

References

Allen, C. W. 1973, Astrophysical quantities, 3rd ed. (London: Athlone press), 37
Baluteau, J.-P., Cox, P., Cernicharo, J., et al. 1997, A&A, 322, L33
Bock, J. J., Hristov, V. V., Kawada, M., et al. 1993, ApJ, 410, L115
Boreiko, R. T., & Betz, A. L. 1995, ApJ, 454, 307
Boreiko, R. T., & Betz, A. L. 1997, ApJ, 111, 409
Brooks, K. J., Whiteoak, J. B., & Storey, J. W. V. 1998, PASA, 15, 202
Brooks, K. J., Cox, P., Schneider, N., et al. 2003, A&A, 412, 751
Cardelli, J. A., Meyer, D. M., Jura, M., & Savage, B. D. 1996, ApJ, 467, 334
Carral, P., Hollenbach, D. J., Lord, S. D., et al. 1994, ApJ, 423, 223
Cartledge, S. I. B., Meyer, D. M., Lauroesch, J. T., & Sofia, U. J. 2001, ApJ, 562, 394
Caux, E., Ceccarelli, C., Castets, A., et al. 1999, A&A, 347, L1
Chan, K.-W., Roellig, T. L., Onaka, T., et al. 2001, ApJ, 546, 273
Clegg, P. E., Ade, P. A. R., Armand, C., et al. 1996, A&A, 315, L38
Colbert, J. W., Malkan, M. A., Clegg, P. E., et al. 1999, A&A, 511, 721
Colgan, S. W., Haas, M. R., Erickson, E. F., et al. 1993, ApJ, 413, 237
Cox, P. 1995, Rev. Mex. Astron. Astrofis., 2, 105
Cox, P., & Bronfman, L. 1995, A&A, 299, 583
Crawford, M. K., Genzel, R., Townes, C. H., & Watson, D. M. 1985, ApJ, 291, 755
de Graauw, T., Lidholm, S., Fitton, B., et al. 1981, A&A, 102, 257
de Graauw, T., Haser, L. N., Beintema, D. A., et al. 1996, A&A, 315, L49
de Jong, T., Dalgarno, A., & Boland, W. 1980, A&A, 91, 68
Draine, B. T. 1990, in The evolution of the interstellar medium, ed. L. Blitz, ASP Conf. Ser., 12, 193
Draine, B. T., & Lee, H.-M. 1984, ApJ, 285, 89
Dwek, E. 1998, ApJ, 501, 643
Erickson, E. F., Colgan, S. W., Simpson, J. P., et al. 1991, ApJ, 370, L69
Feinstein, A. 1995, Rev. Mex. Astron. Astrofis., 285, 89
Fitzpatrick, E. L. 1996, ApJ, 473, L55
Fitzpatrick, E. L. 1997, ApJ, 482, L199
Giannini, T., Nisini, B., Lorenzetti, D., et al. 2000, A&A, 358, 310
Gry, C., Swinyard, B., Harwood, A., et al. 2002, The ISO Handbook volume IV: LWS – The Long Wavelength Spectrometer, Ver. 2.0
Haas, M. R., Hollenbach, D. J., & Erickson, E. F. 1991, ApJ, 374, 555
Habing, H. J. 1968, Bull. Astro. Inst. Netherlands, 19, 421
Hayes, M. A., & Nussbaumer, H. 1984, A&A, 134, 193
Heiles, C. 1994, ApJ, 436, 720
Hollenbach, D. J., & Tielens, A. G. G. M. 1999, Rev. Mod. Phys., 71, 173
Hollenbach, D. J., Takahashi, T., & Tielens, A. G. G. M. 1991, ApJ, 377, 192
Holweger, H. 2001, Solar and galactic composition, ed. R. F. Wimmer-Schweingruber, AIP Conf. Proc., 598, 23
Jones, A. P. 2000, J. Geophys. Res., 105, 10257
Jones, A. P., Tielens, A. G. G. M., Hollenbach, D. J., & Mckee, C. F. 1994, ApJ, 433, 797
Jones, A. P., Tielens, A. G. G. M., & Hollenbach, D. J. 1996, ApJ, 469, 740
Kaufman, M. J., Wolfire, M. G., Hollenbach, D. J., & Luhman, M. L. 1999, ApJ, 527, 795
Keenan, F. P., Conlon, E. S., & Rubin, R. H. 1994, ApJ, 434, 811
Kessler, M. F., Steinz, J. A., Anderegg, M. E., et al. 1996, A&A, 315, L27
Kraemer, K. E., Jackson, J. M., & Lane, A. P. 1998, ApJ, 503, 785
Launey, J. M., & Roueff, E. 1977, J. Phys. B, Atom. Molec. Phys., 10, 879
Le Bourlot, J., Pineau des Forêts, G., Roueff, E., & Flower, D. R. 1993, A&A, 276, 233
Leech, K., Kester, D., Shipman, R., et al. 2002, The ISO Handbook volume V: SWS – The Short Wavelength Spectrometer, Ver. 2.0
Li, W., Evans, N. J. II, Jaffe, D. T., van Dishoeck, E. F., & Thi, W.-F. 2002, ApJ, 568, 242
Liseau, R., White, G. J., Larsson, B., et al. 1999, A&A, 344, 342
Lord, S. D., Hollenbach, D. J., Haas, M. R., et al. 1996, ApJ, 465, 703
Makiuti, S., Shibai, H., Okuda, H., et al. 1996, PASJ, 48, L71
Makiuti, S., Shibai, H., Nakagawa, T., et al. 2002, A&A, 382, 600
Malhotra, S., Kaufman, M. J., Hollenbach, D., et al. 2001, ApJ, 561, 766

Martín-Hernández, N. L., Peeters, E., Morisset, C., et al. 2002, A&A, 381, 606
Mathis, J. S. 1990, ARA&A, 28, 37
Matsuhara, H., Nakagawa, T., Shibai, H., et al. 1989, ApJ, 339, L69
Meixner, M., Haas, M. R., Tielens, A. G. G. M., Erickson, E. F., & Werner, M. 1992, ApJ, 390, 499
Mendoza, C. 1983, in Planetary Nebulae, ed. D. R. Flower, IAU Symp., 103, 143
Mizutani, M., Onaka, T., & Shibai, H. 2002, A&A, 382, 610 (Paper I)
Mochizuki, K., & Nakagawa, T. 2000, ApJ, 535, 118
Morris, P. W., Waters, L. B. F. M., Barlow, M. J., et al. 1999, Nature, 402, 502
Nakagawa, T., Yui, Y. Y., Doi, Y., et al. 1998, ApJS, 115, 259
Negishi, T., Onaka, T., Chan, K.-W., & Roellig, T. L. 2001, A&A, 375, 566
Nussbaumer, H., & Storey, P. J. 1981, A&A, 96, 91
Okada, Y., Onaka, T., Shibai, H., & Doi, Y. 2003, A&A, 412, 199
Onaka, T., 2000, in ISAS report SP-14, Mid- and Far-Infrared Astronomy and Future Space Missions, ed. T. Matsumoto, & H. Shibai, 83
Osterbrock, D. E. 1989, Astrophysics of gaseous nebulae and active galactic nuclei (Mill Valley: University Science Books)
Peeters, E., Martín-Hernández, N. L., Damour, D., et al. 2002, A&A, 381, 571
Poglitsch, A., Krabee, A., Madden, S., et al. 1995, ApJ, 454, 293
Poglitsch, A., Herrmann, F., Genzel, R., et al. 1996, ApJ, 462, L43
Rathborne, J. M., Burton, M. G., Brooks, K. J., et al. 2002, MNRAS, 331, 85
Salama, A. 2000, in ESA SP-455, ISO Beyond Point Sources: Studies of Extended Infrared Emission, ed. R. J. Laureijs, K. Leech, & M. F. Kessler, 7
Savage, B. D., & Sembach, K. R. 1996, ARA&A, 34, 279
Seab, C. G., & Shull, J. M. 1983, ApJ, 275, 652
Sembach, K. R., Howk, J. C., Ryans, R. S. I., & Keenan, F. P. 2000, ApJ, 528, 310
Shibai, H., Okuda, H., Nakagawa, T., et al. 1991, ApJ, 374, 522
Shibai, H., Okuda, H., Nakagawa, T., et al. 1996, PASJ, 48, L123
Smith, N., Egan, M. P., Carey, S., et al. 2000, ApJ, 532, L145
Sofia, U. J., Cardelli, J. A., Guerin, K. P., & Meyer, D. M. 1997, ApJ, 482, L105
Stacey, G. J., Geis, N., Genzel, R., et al. 1991, ApJ, 373, 423
Stacey, G. J., Jaffe, D. T., Geis, N., et al. 1993, ApJ, 404, 219
Stolovy, S. R., Herter, T., Gull, G. E., et al. 1995, in Airborne Astronomy Symp. on the Galactic Ecosystem: From gas to stars to dust, ed. M. R. Haas, J. A. Davidson, & E. F. Erickson, ASP Conf. Ser., 73, 469
Tauber, J. A., Tielens, A. G. G. M., Meixner, M., & Goldsmith, P. F. 1994, ApJ, 422, 136
Tielens, A. G. G. M. 1998, ApJ, 499, 267
Tielens, A. G. G. M., & Hollenbach, D. 1985, ApJ, 291, 722
Unger, S. J., Clegg, P. E., Stacey, G. J., et al. 2000, A&A, 355, 885
Vastel, C., Caux, E., Ceccarelli, C., et al. 2000, A&A, 357, 994
Vastel, C., Spaans, M., Ceccarelli, C., Tielens, A. G. G. M., & Caux, E. 2001, A&A, 376, 1064
Vázquez, R. A., Baume, G., Feinstein, A., & Prado, P. 1996, A&AS, 75
Walborn, N. R. 1973, ApJ, 179, 517
Walborn, N. R. 1995, Rev. Mex. Astron. Astrofis., 2, 51
Walborn, N. R., Danks, A. C., Sembach, K. R., et al. 1998, ApJ, 492, L169
Walborn, N. R., Danks, A. C., Vieira, G., & Landsman, W. B. 2002, ApJS, 140, 407
Watson, D. M. 1984, in Galactic and Extragalactic Infrared Spectroscopy, ed. M. F. Kessler, & J. P. Phillips (Dordrecht: Reidel), 195
Wolfire, M. G., Tielens, A. G. G. M., & Hollenbach, D. 1990, ApJ, 358, 116
Wright, E. L., Mather, J. C., Bennet, C. L., et al. 1991, ApJ, 381, 200
Young Owl, R. C., Meixner, M. M., Fong, D., et al. 2002, ApJ, 578, 885
Yui, Y. Y., Nakagawa, T., Doi, Y., et al. 1993, ApJ, 419, L37
Zhang, X., Lee, Y., Bolatto, A., & Stark, A. A. 2001, ApJ, 553, 274